Binding Preferences of the Tribenzylidenemethane Ligand in High-Oxidation-State Tantalum Complexes

George Rodriguez,[†] John P. Graham,[§] W. Donald Cotter,[‡] Caroline K. Sperry,[†] Guillermo C. Bazan,*[,||] and Bruce E. Bursten*[,§]

Contribution from the Department of Chemistry, University of Rochester, Rochester, New York, 14627-0216, Department of Chemistry, Mount Holyoke College, South Hadley, Massachusetts 01075, Department of Chemistry, The Ohio State University, Columbus, Ohio 43210, and Department of Chemistry, The University of California, Santa Barbara, California 93106

Received May 11, 1998

Abstract: Reaction of $Li_2(TBM)(TMEDA)_2$ (TBM = tribenzylidenemethane) with $TaMe_3Cl_2$ gives (TBM)$TaMe_3$ (**1**) in 44% yield. Structural characterization of the (*tert*-Bu-TBM)$TaMe_3$ derivative **2** shows an eclipsed orientation of the $TaMe_3$ tripod relative to the inner core of the TBM ligand. Treatment of (TBM)$TaMe_3$ with $ZnCl_2$ cleanly replaces one methyl ligand for chloride to give (TBM)$TaMe_2Cl$ (**3**) which is a versatile precursor to (TBM)Ta-based complexes. Addition of $LiNPh_2$ to **3** gives (TBM)$TaMe_2(NPh_2)$ (**4**). Structural characterization reveals that both **3** and **4** have eclipsed frameworks. Metallocene-mimics are accessible by reacting LiCp (Cp = C_5H_5), LiCp* (Cp* = C_5Me_5), LiCp′ (Cp′ = C_5H_4Me), or LiFlu (Flu = fluorenyl) with **3** to give Cp(TBM)$TaMe_2$ (**5**), Cp*(TBM)$TaMe_2$ (**6**), Cp′(TBM)$TaMe_2$ (**7**), and Flu(TBM)$TaMe_2$ (**8**), respectively. The solid-state structures of **5**, **7**, and **8** display gross molecular geometries similar to those of group 4 metallocenes. Complex **3** reacts with tris(pyrazolylborate) or bis(pyrazolylborate) salts. Thus, [HB(pz)$_3$](TBM)$TaMe_2$ (**9**), [HB(3,5-Me_2-1-pz)$_3$](TBM)$TaMe_2$ (**10**), and [H_2B(pz)$_2$](TBM)$TaMe_2$ (**11**) are obtained from Na[HB(pz)$_3$], K[HB(3,5-Me_2-1-pz)$_3$], and K[H_2B(pz)$_2$], respectively. Structural characterization of **9**, **10**, and **11** shows that TBM can adopt a continuum of bonding modes, from η^4 to η^2, depending on the steric hindrance around the metal center. The TMM ligand participates in hydrogenation and insertion reactions, indicating that TMM is a weak ancillary ligand. Combining **6**, **7**, or **8** with MAO results in short-lived ethylene polymerization catalysts. Finally, an electronic description of the model complex (TMM)$TaMe_3$ is developed to account for the eclipsed molecular structures of **1**−**4**. A comparison against the orbital description of staggered (TMM)$Fe(CO)_3$ is also made.

Introduction

There is considerable current interest in finding ligands that serve as cyclopentadienyl substitutes for early transition-metal complexes.[1] This effort is promoted, in part, by the expectation of developing new homogeneous olefin polymerization catalysts. In this respect, group 4 metallocenes remain the most thoroughly studied class of complexes (i.e., Cp_2ZrMe_2, Cp = C_5H_5; or Cp*$_2$-$ZrCl_2$, Cp* = C_5Me_5).[2,3] Non-Cp ligands can be used in the design of unique catalysts. For example, activated forms of [(η^5-C_5Me_4)$SiMe_2$(η^1-$NCMe_3$)]$TiMe_2$ can incorporate substantial amounts of α-olefins into growing polyethylene chains and [(Ar)N(CH_2)$_3$N(Ar)]$TiMe_2$ with B(C_6F_5)$_3$ can polymerize α-olefins in a living fashion.[4,5]

Group 5 metallocene mimics that can be used as Ziegler−Natta catalyst precursors have been sought for some time, since classical vanadium catalysts are known to have excellent activities.[6] One strategy takes advantage of *dianionic* 6 π electron donors to create a metallocene-like molecular structure and maintain a formally d^0 metal center:

Despite structural and electronic similarity to well-known group 4 catalysts, tantalum compounds have thus far proven less effective. Dianionic boron cages serve as 6π donor ligands in (C_5H_4Me)[$C_2B_9H_{11}$]$TaMe_2$ and the benzyne complex Cp[Et_2-

[†] University of Rochester.
[‡] Mount Holyoke College.
[§] The Ohio State University.
[||] The University of California−Santa Barbara.

(1) Recent overviews: (a) Bochmann, M. *J. Chem. Soc., Dalton Trans.* **1996**, 255. (b) Sperry, C. K.; Rodriguez, G.; Bazan, G. C. *J. Organomet. Chem.* **1997**, *548*, 1.

(2) (a) Brintzinger, H. H.; Fischer, D.; Mülhaupt, R.; Rieger, B.; Waymouth, R. M. *Angew. Chem., Int. Ed. Engl.* **1995**, *34*, 1143. (b) *Ziegler Catalysts*; Fink, G., Mülhaupt, R., Brintzinger, H. H., Eds.; Springer-Verlag: Berlin, 1995.

(3) Jordan, R. F. *Adv. Organomet. Chem.* **1991**, *32*, 325.

(4) (a) Lai, S.; Wilson, J. R.; Knight, G. W.; Stevens, J. C.; Chum, P. S. U.S. Patent 5,272,236. (b) Shapiro, P. J.; Cotter, W. D.; Schaefer, W. P.; Labinger, J. A.; Bercaw, J. E. *J. Am. Chem. Soc.* **1994**, *116*, 4623.

(5) Scollard, J. D.; McConville, D. H. *J. Am. Chem. Soc.* **1996**, *118*, 10008.

(6) (a) Haszeline, R. N.; Hyde, T. G.; Tait, P. J. T. *Polymer* **1973**, *14*, 215. (b) Haszeline, R. N.; Hyde, T. G.; Tait, P. J. T. *Polymer* **1973**, *14*, 221. (c) Haszeline, R. N.; Hyde, T. G.; Tait, P. J. T. *Polymer* **1973**, *14*, 224. (d) Doi, Y.; Tokuhiro, N.; Suzuki, S.; Soga, K. *Makromol. Chem. Rapid Commun.* **1987**, *8*, 285. (e) Fernandez, D.; Fernandez, C.; Rodriguez, J. D.; Arberola, A. *Eur. Polym. J.* **1989**, *25*, 1309.

10.1021/ja981640t CCC: $15.00
Published on Web 11/20/1998

$C_2B_4H_4]Ta(\eta^2\text{-}C_6H_4)(PMe_3)$. Transformation of these precursors into active catalysts has not been reported.[7,8] Polymerization is observed when the borollide complex $Cp^*[C_4H_4B-N(CHMe_2)_2]TaMe_2$ is treated with MAO and ethylene, but the propagating species decompose rapidly at polymerization temperatures.[9] Living olefin polymerization has been reported using complexes of the type $Cp^*(\eta^4\text{-butadiene})M(Me)_2$ (M = Ta, Nb) with MAO at low temperatures.[10] We recently reported zirconium and tantalum complexes containing the tribenzylidenemethane (TBM) ligand. Like its simpler relative, trimethylenemethane (TMM), TBM can donate up to 6 π electrons, and for this reason it may be viewed as a dianionic analogue of the cyclopentadienyl ligand.[11,12]

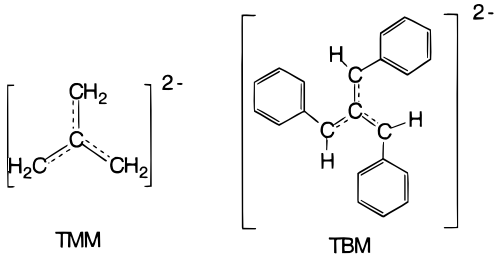

In this contribution we present a detailed study of TBM complexes of tantalum. The primary aim is to obtain a clearer picture of the Ta−TBM bonding interaction. We show that piano-stool complexes adopt the eclipsed conformation and that this preference has an electronic origin. Also, a range of pyrazolylborate complexes is reported in which TBM assumes a continuum of coordination modes. Thus, TBM is able to accommodate the electronic and steric requirements of the metal through subtle but significant changes in its coordination geometry. Reactivity studies show that, at least in the case of tantalum, the TBM ligand is more reactive than Cp and less effective at stabilizing catalytic species.

Results and Discussion

Synthesis and Structural Characterization. The slow addition of $Li_2(TBM)(TMEDA)_2$ or Li_2(*tert*-Bu-TBM)$(TMEDA)_2$ to $TaMe_3Cl_2$ results in the formation of $(TBM)TaMe_3$ (**1**) and (*tert*-Bu-TBM)$TaMe_3$ (**2**), respectively (eq 1).[11] Isolation of **1** requires efficient removal of TMEDA by xylene condensation−evaporation cycles on the crude reaction mixture. Extraction with benzene affords **1** as a thermally stable orange solid. Compound **2** may be isolated in a similar manner by performing the condensation−evaporation cycles with octane. Removal of TMEDA is important for separating $LiCl(TMEDA)_x$ byproducts. Higher field chemical shifts are characteristic of the coordinated ligand (i.e., δ 4.41 for the methylene protons in **1** relative to δ 5.21 for $Li_2(TBM)(TMEDA)_2$. In **2** the three benzylic arms are chemically inequivalent, but a single resonance is observed (δ 0.7) for the three Me groups as a result of rapid TBM rotation on the NMR time scale at room temperature. The reactions in eq 1 are remarkable, considering the ease of reduction of Me_3TaCl_2.

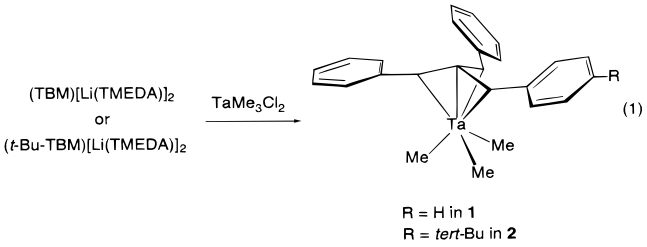

Treating **1** with $ZnCl_2$ in THF/C_6H_6 results in an orange to red color change. Analysis by ^1H NMR spectroscopy reveals that the product contains a π-bound TBM and two inequivalent Ta−Me groups (δ 0.91 and 0.82). These spectroscopic features together with elemental analysis are consistent with the formation of $(TBM)TaMe_2Cl$ (**3**) (eq 2).[11] Other Lewis acids, such as $AlCl_3$ or $B(C_6F_5)_3$ in CH_2Cl_2, are also effective in forming **3** from **1**, but do so at slower rates. Compound **3** is a versatile starting material for preparing a variety of TBM-containing Ta complexes (vide infra).

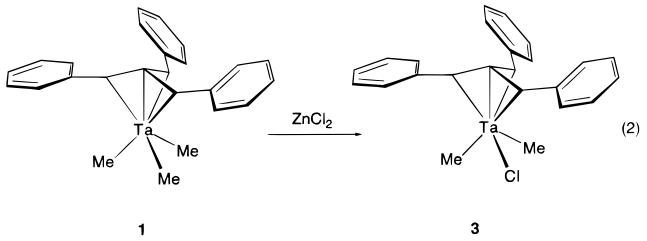

The solid-state structures of **2** and **3** were previously determined by X-ray crystallography.[11] Tantalum is seven-coordinate with a "domed" TBM framework. The three phenyl rings are in a propeller-like arrangement. The overall molecular geometry of **2** and **3** is analogous to that of piano-stool compounds ($CpMX_3$),[13] where TBM replaces Cp as the "seat" of the stool. An unexpected molecular characteristic is the eclipsed, trigonal prismatic-like arrangement of the TBM framework (neglecting TBM's inner carbon) relative to the $TaMe_3$ and $TaMe_2Cl$ tripods. By contrast, the late metal counterpart $(TMM)Fe(CO)_3$ prefers a staggered geometry.[14]

To probe further the relative energies of the different conformations, we introduced a sterically demanding π donor ligand which might enforce a staggered (quasi-octahedral) geometry. $(TBM)Ta(NPh_2)Me_2$ (**4**) was therefore prepared, via

(7) (a) Uhrhammer, R.; Crowther, D. J.; Olsen, J. D.; Swenson, D. C.; Jordan, R. F. *Organometallics* **1992**, *11*, 3098. (b) Uhrhammer, R.; Su, Y. X.; Swenson, D. C.; Jordan, R. F. *Inorg. Chem.* **1994**, *33*, 4398.

(8) Hausknecht, K. L.; Stockman, K.; Sabat, M.; Finn, M. G.; Grimes, R. N. *J. Am. Chem. Soc.* **1995**, *117*, 1163.

(9) Bazan, G. C.; Donnelly, S.; Rodriguez, G. *J. Am. Chem. Soc.* **1995**, *117*, 2671.

(10) (a) Mashima, K.; Nakamura, A. *J. Organomet. Chem.* **1995**, *500*, 261. (b) Mashima, K.; Fujikawa, S.; Tanaka, Y.; Urata, H.; Toshiyuki, O.; Tanaka, E.; Nakamura, A. *Organometallics* **1995**, *14*, 2633. (c) Okamoto, T.; Yasuda, H.; Nakamura, A.; Kai, Y.; Kanehisa, N.; Kasai, N. *Organometallics* **1988**, *7*, 2266.

(11) Rodriguez, G.; Bazan, G. C. *J. Am. Chem. Soc.* **1995**, *117*, 10155.

(12) (a) Bazan, G. C.; Rodriguez, G.; Cleary, B. P. *J. Am. Chem. Soc.* **1994**, *116*, 2177. (b) Bazan, G. C.; Rodriguez, G. *J. Am. Chem. Soc.* **1997**, *119*, 343.

(13) Examples of piano stool compounds can be found in general organometallic texts: (a) Elschenbroich, C., Salzer, A. *Organometallics*; VCH: New York, 1989. (b) Collman, J. P.; Hegadus, L. S.; Norton, J. R.; Finke, R. G. *Principles and Applications of Organotransition Metal Chemistry*; University Science Books: Mill Valley, CA, 1987. (c) *Comprehensive Organometallic Chemistry II*; Abel, E. W., Stone, F. G., Wilkinson, G., Eds.; Pergamon: Oxford, 1995; Vol. 2.

(14) (a) Girard, L. Baird, M. C. *J. Organomet. Chem.* **1993**, *444*, 143. (b) Albright, T. A.; Hofmann, P.; Hoffmann, R. *J. Am. Chem. Soc.* **1977**, *99*, 7546. (c) Almenningen, A.; Haaland, A.; Wahl, K. *Acta Chem. Scand.* **1969**, *23*, 1145. (d) Churchill, M. R.; DeBoer, B. G. *Inorg. Chem.* **1973**, *12*, 525. (e) O'Callaghan, K. A. E.; Brown, S. J.; Page, J. A.; Baird, M. C.; Richards, T. C.; Geiger, W. E. *Organometallics* **1991**, *10*, 3119. (f) Churchill, M. R.; Gold, K. *Inorg. Chem.* **1969**, *8*, 401.

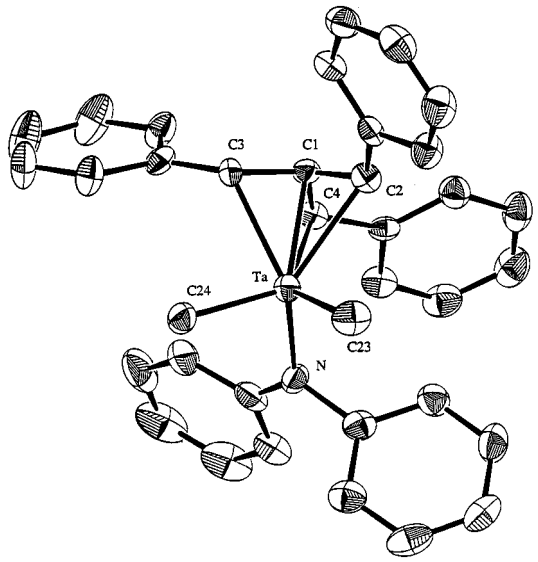

Figure 1. ORTEP drawing of **4**. Ellipsoids are drawn at 30% probability. Hydrogen atoms are omitted for clarity.

Table 1. Selected Bond Distances and Angles for **4**

atoms	distance (Å)	atoms	angles (deg)
Ta−C(1)	2.249(5)	C(23)−Ta−C(24)	91.3(3)
Ta−C(2)	2.414(6)	C(2)−C(1)−C(3)	115.2(5)
Ta−C(3)	2.325(6)	C(2)−C(1)−C(4)	117.3(5)
Ta−C(4)	2.405(5)	C(3)−C(1)−C(4)	112.7(5)
Ta−C(23)	2.139(6)		
Ta−C(24)	2.181(6)		
Ta−N	2.006(5)		

treatment of **3** with 1 equiv of $LiNPh_2$ (eq 3). Compound **4** is a moderately air-sensitive, thermally stable, red-orange crystalline solid.

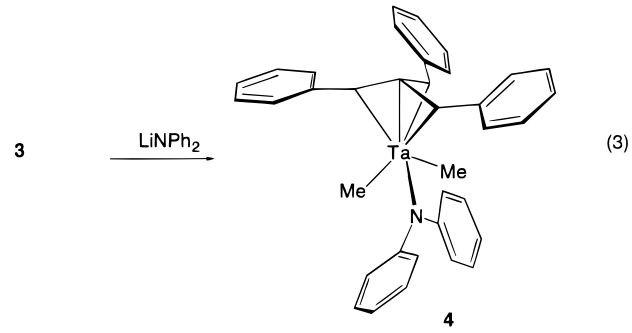

Single crystals suitable for crystallography were obtained by allowing a diethyl ether solution of **4** to evaporate slowly. The result of this study is shown in Figure 1, and selected bond lengths and angles are given in Table 1. The short Ta−N distance (2.006(5) Å)[15] and sp^2-hybridized N atom suggest a Ta−N π bond. As shown in Figure 1, the eclipsed conformation is maintained. Compound **4** is a structural analogue of $CpZrCl_2(NR_2)$.[16] Note that in **4**, the phenyl groups of the amido ligand are rotated away from the benzylidene arms of TBM to avoid steric contacts.

Treating **3** with CpLi or Cp*Li affords $Cp(TBM)TaMe_2$ (**5**) and $Cp^*(TBM)TaMe_2$ (**6**), respectively (eq 4). These reactions are nearly quantitative by ^1H NMR spectroscopy. However, the Cp* derivative is isolated in only 50% yield as a red oil which is difficult to crystallize. In contrast, $Cp(TBM)TaMe_2$ has limited solubility and is isolated by performing the reaction in THF and collecting the resulting air-stable red precipitate.

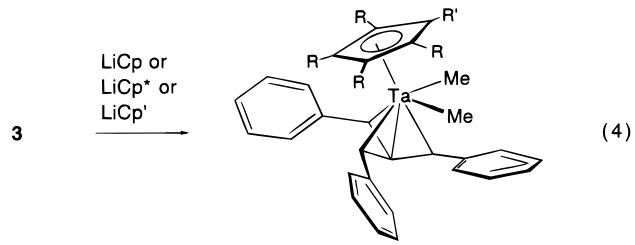

5 for R = R' = H
6 for R = R' = Me
7 for R = H, R' = Me

The molecular structures of **5** and **6** were sought to elucidate the Ta−TBM relationship within a metallocene-like environment. In the case of **6**, suitable crystals could not be obtained. Crystals of **5** were obtained, but its solid-state structural characterization revealed two independent molecules on a 3-fold axis with a disorder involving the methyl and Cp ligands. Anisotropic refinement of the Cp and methyl carbons was not possible, and detailed intramolecular structural parameters could not be obtained.[17]

To resolve the uncertainties raised above, two derivatives were prepared and structurally characterized: $Cp'(TBM)TaMe_2$ (**7** in eq 4) by reaction of **3** with LiCp′ (Cp′ = C_5H_4Me), and $Flu(TBM)TaMe_2$ (**8**, in eq 5) by reaction of **3** with LiFlu (Flu = fluorenyl).

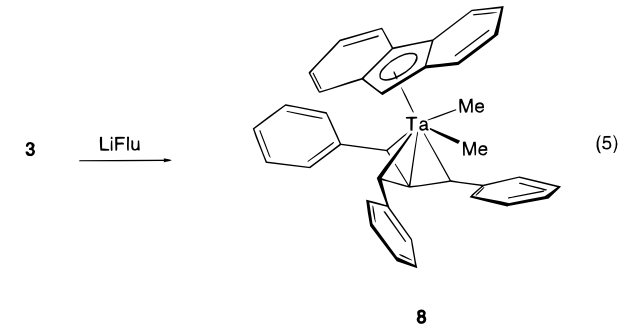

8

Figures 2 and 3 show ORTEP illustrations of **7** and **8**, respectively, with selected bond distances and angles given in Table 2. The two compounds resemble a bent group 4 metallocene with *syn*-η^4 bound TBM ligands. The C_l−Ta−Cp_{cent} angles in **7** (134.8(8) °) and **8** (135.7(6) °) are very similar to the Cp_{cent}−Zr−Cp_{cent} angle in Cp_2ZrCl_2 (132.5°)[18] (see Table 2 for angles and definition of C_l). The bonding of the fluorenyl ligand to Ta in **8** is of particular interest. The Ta−C(23) distance (2.336(4) Å) is substantially shorter than those of Ta−C(29) (2.717(4) Å) and Ta−C(30) (2.650(3) Å), implying that the fluorenyl ligand in **8**, at least in the solid state, is close to assuming an η^3 geometry.[19]

The electronic properties of Cp′ and Cp are similar, and the structure of **7** may be used as a model for that of **5**. The symmetrical binding of the TBM ligand in **7** (Ta−C distances of 2.468(7), 2.336(6), and 2.477(6) Å) may be compared to the

(15) Schaller, C. P.; Wolczanski, P. T. *Inorg. Chem*. **1993**, *32*, 131.
(16) Pupi, R. M.; Coalter, J. N.; Petersen, J. L.; *J. Organomet. Chem*. **1995**, *497*, 17.
(17) Schaefer, W. P.; Marsh, R. E.; Rodriguez. G.; Bazan, G. C. *Acta Crystallogr*. **1996**, *B52*, 465.
(18) Hunter, W. E.; Hrncir, D. C.; Bynum, R. V.; Penttila, R. A.; Atwood, J. L. *Organometallics* **1983**, *2*, 750.
(19) Kowala, C.; Wunderlich, J. A. *Acta Crystallogr*. (*Sect. B*.) **1976**, *32*, 820.

Table 2. Selected Bond Distances (Å) and Angles (deg) for **5**,[a] **7**, and **8**[b]

complex	Me_L	Me_R	C_I	C_T	C_L	C_R	L_{Cp}−Ta−C_I
$Cp(TBM)TaMe_2$ (**5**)	2.2445(31)	2.2445(31)	2.2943(14)	2.429(8)	2.429(8)	2.429(8)	131.5(9)
$Cp'(TBM)TaMe_2$ (**7**)	2.190(7)	2.220(7)	2.259(6)	2.468(7)	2.336(6)	2.477(6)	134.8(8)
$Flu(TBM)TaMe_2$ (**8**)	2.174(4)	2.168(4)	2.217(3)	2.431(3)	2.364(4)	2.525(3)	135.7(6)

[a] Previously reported (see ref 11). [b] The atom designators are defined by the following figure (L_{Cp} = Cp, Cp; or Flu).

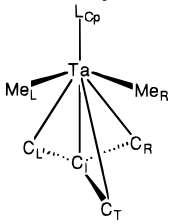

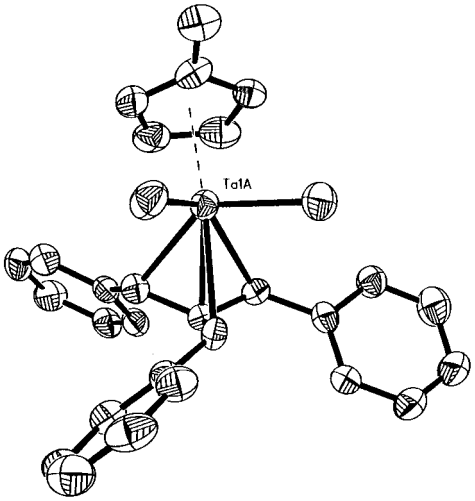

Figure 2. ORTEP drawing of **7**. Ellipsoids are drawn at 30% probability. Hydrogen atoms are omitted for clarity.

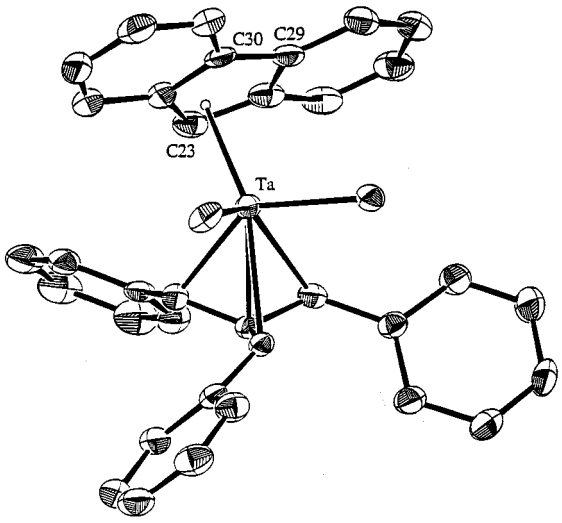

Figure 3. ORTEP drawing of **8**. Ellipsoids are drawn at 30% probability. Hydrogen atoms are omitted for clarity.

binding of TBM in the isoelectronic zirconium complex $[Cp^*(TBM)ZrCl_2]^-$.[11] In the anion the two benzyl carbons syn to the Cp* ligand show markedly tighter binding than the single anti carbon (2.48(1) Å and 2.45(1) Å vs 2.78(1) Å). The trans effect of the Cp* ligand creates a ground state in which the TBM ligand approximates an ene-diyl fragment. The internal C−C bond lengths show a long-long−short pattern as well (1.47(1) Å and 1.42(1) Å vs 1.38(1) Å). As we will show below, the presence of bulky tris(pyrazolylborate) ligands

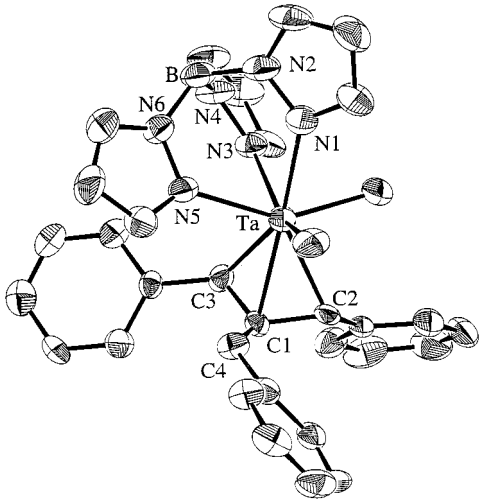

Figure 4. ORTEP drawing of **9**. Ellipsoids are drawn at 30% probability. Hydrogen atoms are omitted for clarity. Important distances (in Å): Ta−C(1), 2.345(9); Ta−C(2), 2.237(8); Ta−C(3), 2.28(1); Ta−C(4), 2.896(4); C(1)−C(2), 1.47(1); C(1)−C(3), 1.45(1); C(1)−C(4), 1.39(1).

progressively accentuates the deviation from symmetric η^4 binding to a strictly η^2-bidentate form.

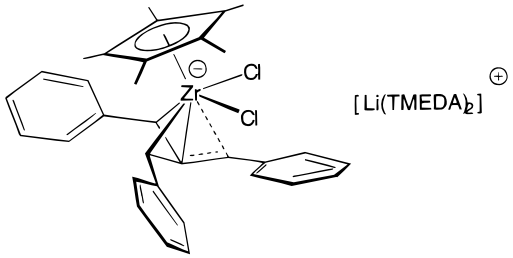

One equivalent of **3** reacts with $Na[HB(pz)_3]$ ($HB(pz)_3$ = tris(pyrazolylborate)) in tetrahydrofuran to give $[HB(pz)_3](TBM)TaMe_2$ (**9**) in 60% yield (eq 6). The solid-state structure (Figure

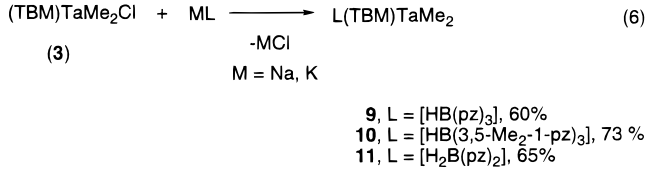

4) reveals that **9** contains a three-coordinate $HB(pz)_3$ ligand and a distorted TBM ligand (d(Ta−C(4)) = 2.895(4) Å vs d(Ta−

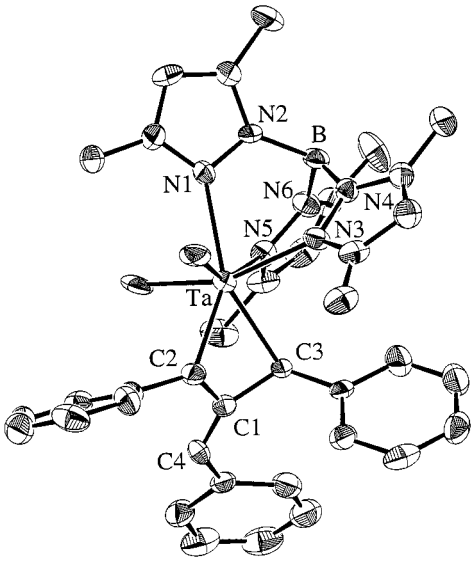

Figure 5. ORTEP drawing of **10**. Ellipsoids are drawn at 30% probability. Hydrogen atoms are omitted for clarity. Important distances (in Å): Ta−C(1), 2.675(4); Ta−C(2), 2.251(8); Ta−C(3), 2.287(8); Ta−C(4), 3.842(5); C(1)−C(2), 1.47(1); C(1)−C(3), 1.49(1); C(1)−C(4), 1.36(1).

C(1)) = 2.345(9) Å, d(Ta−C(2)) = 2.357(8) Å and d(Ta−C(3)) = 2.28(1) Å). For **9** in the solid state the TBM ligand is η^3-bound.

Compound [HB(3,5-Me_2-1-pz)$_3$](TBM)$TaMe_2$ (**10**) is obtained from **3** and K[HB(3,5-Me_2-1-pz)$_3$] in 73% yield. The X-ray structure of **10** is shown in Figure 5. The larger size of the [HB(3,5-Me_2-1-pz)$_3$] ligand relative to [HB(pz)$_3$] changes the Ta−TBM relationship. Relative to compound **9**, there is a reduction in the Ta−C(2) (2.251(8) Å) and Ta−C(3) (2.287(8) Å) bond distances, while the Ta−C(1) (2.675(4) Å) and Ta−C(4) (3.842(5) Å) distances are significantly longer. Orbital overlap between Ta and C(1) and C(4) can be ruled out based on these metrical parameters, and as a result TBM is best described as η^2-bound. The contraction of the C(2)−C(1)−C(3) angle from 110.8(8)° in **9** to 104.5(7)° in **10** is also notable. Furthermore, the sum of angles about C(1) (359.2(9) °) in **10** is consistent with sp^2 hybridization. This Ta−TBM interaction is best described as an exo-benzylidene(α,α′-diphenyl)tantalacyclobutane fragment.[20]

The reaction of **3** and K[H_2B(pz)$_2$] affords [H_2B(pz)$_2$](TBM)$TaMe_2$ (**11**). Figure 6 shows the crystallographically determined coordination environment of tantalum. The TBM core in **11** is tightly bound as shown by the Ta−C(1) (2.282(5) Å), Ta−C(2) (2.509(5) Å), Ta−C(3) (2.365(5) Å), and Ta−C(4) (2.446(5) Å) bond distances and adopts the typical "domed" shape with the inner carbon closest to the metal. The TBM framework is pseudoaxial to one of the pyrazolyl arms (C(1)−Ta−N(1) = 177.8(2)°) and staggered relative to the other three ligands. The boatlike puckering of the six-membered chelating ring [Ta(1), B(1), and N(1)−N(4)], and the short Ta(1)−B(1) distance (2.900(5) Å) suggest a three-center, two-electron B−H−Ta bond. These structural features are nearly identical to those found in (H(μ-H)B(1-pz)$_2$)$TaMe_3Cl$ (Ta−B = 2.897(12) Å)[21] and Cp(H(μ-H)B(1-pz)$_2$)$ZrCl_2$ (Zr−B = 2.957 (5) Å).[22] The

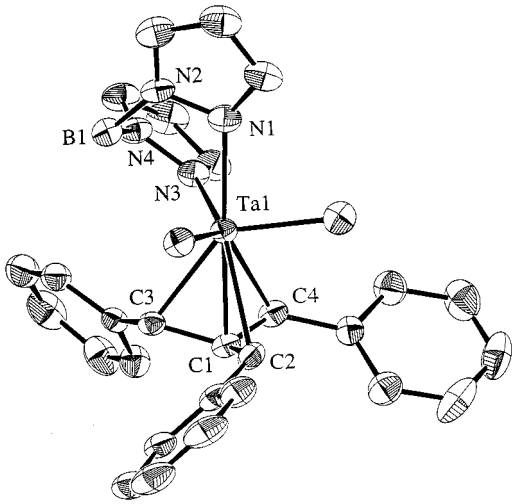

Figure 6. ORTEP drawing of **11**. Ellipsoids are drawn at 30% probability. Hydrogen atoms are omitted for clarity. Important distances (in Å): Ta(1)−C(1), 2.282(4); Ta(1)−C(2), 2.509(5); Ta(1)−C(3), 2.365(5); Ta(1)−C(4), 2.446(5); C(1)−C(2), 1.412(7); C(1)−C(3), 1.462(7); C(1)−C(4); 1.418(7).

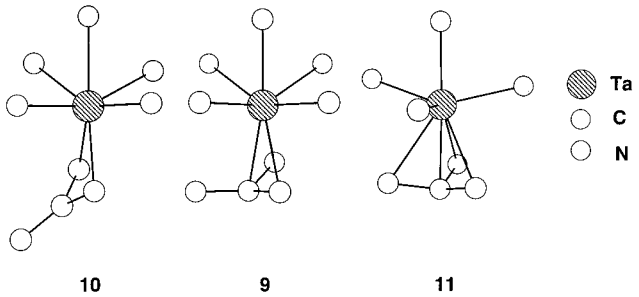

Figure 7. Coordination sphere of Tantalum in **10**, **9**, and **11**.

infrared spectrum of **11** in tetrahydrofuran contains absorptions at 2484 cm^{-1} (terminal B−H) and 2139 cm^{-1} (bridging B−H−Ta). These bands confirm that the Ta−H−B interaction is also present in solution and that tantalum is nine-coordinate as shown below.

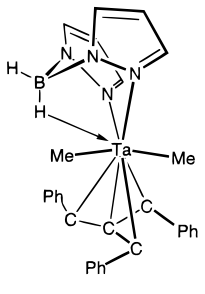

(**11**)

The relative Ta−TBM interactions in **9**−**11** are easily compared by inspecting the coordination sphere at tantalum (Figure 7). Replacing [HB(3,5-Me_2-1-pz)$_3$] (cone angle of 224°) with [HB(pz)$_3$] (cone angle of 184°)[23] reduces the steric envelope around Ta. The more open environment around **9** allows TBM to more closely approach the metal. The η^3 bonding mode of TBM, coupled with the π overlap between C(1) and C(4) observed in **9** resists a simple valence-bond description. We propose the combination of resonance structures **A** and **B** in Scheme 1 to account for the observed molecular

(20) For an example of an η^2 complex of TMM, $Cp^*_2Zr(\eta^2$-TMM), see: Herberich, G. E.; Kreuden, C.; Englert, U. *Angew. Chem., Int. Ed. Engl.* **1994**, *33*, 2465.

(21) Reger, D, L.; Swift, C. A.; Lebioda, L. *J. Am. Chem. Soc.* **1983**, *105*, 5343.

(22) Reger, D. L.; Mahtab, R.; Baxter, J. C.; Lebioda, L. *Inorg. Chem.* **1986**, *25*, 2046.

(23) For a recent review of poly(pyrazolyl)borate chemistry refer to: Trofimenko S. *Chem. Rev.* **1994**, *93*, 943.

Scheme 1

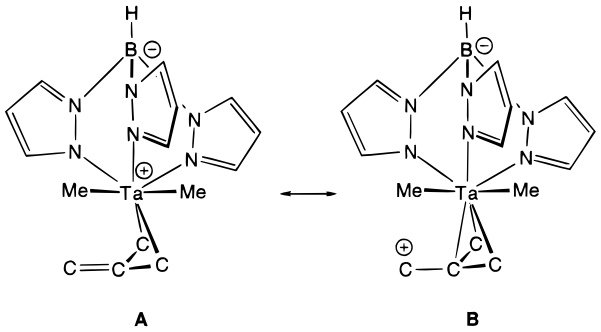

geometry. Exchanging $[HB(pz)_3]$ for $[H_2B(pz)_2]$ increases electron demand at the metal and opens a coordination site. As a result the TBM ligand in **11** can coordinate via four carbons, donating a total of six π electrons to the metal.

Solution characterization by ^{1}H NMR spectroscopy provides information complementary to the solid-state data. The temperature dependence of the signals for the three benzylidene arms can be used to estimate the rate of TBM rotation. In the case of **9**, the three arms are equivalent and there is no evidence of signal broadening, even at temperatures as low as −90 °C. For **10**, these three signals remain inequivalent (δ7.34, 2.13, 2.00) and do not merge, even after heating to 80 °C. Thus, a static structure is observed for **10** relative to the ^{1}H NMR time scale.[24] In the case of **11**, three distinct benzylidene signals (δ 5.75, 5.06, 4.38) coalesce into a sharp singlet at temperatures above 5 °C. The fluxional exchange in **11** was modeled by line shape analysis giving $\Delta H = 11(1)$ kcal/mol and $\Delta S = 4.0(0.6)$ eu.[25]

The different dynamic ^{1}H NMR spectra of **9** and **10**, which have similar geometries except for the TBM binding mode, may be understood in the following manner. In order for TBM rotation to occur in **10**, the exo-benzylidene arm needs to coordinate forming an η^4-TBM intermediate. The steric hindrance of the $[HB(3,5\text{-}Me_2\text{-}1\text{-}pz)_3]$ ligand raises the energy of this η^4 intermediate. Inspection of the molecular frameworks in Figure 7 suggests that formation of the required η^4-TBM intermediate would be facile for **9**, resulting in faster rates of exchange.

Reactivity. In this section we report on the reactivity of TBM−Ta metallocene mimics. Of special interest are the differences between complexes containing the TBM−Ta framework and the isoelectronic Cp−Zr counterpart.

Bercaw and co-workers originally reported the synthesis of $Cp^*(TMM)TaMe_2$ (**12**).[26] Activation of **12** to a reactive 14-electron species, $[Cp^*(TMM)TaMe]^+$, was initially attempted. No evidence of polyethylene formation was observed when a solution of **12** and MAO ([Al]/[Ta] = 800) was exposed to 1 atm of ethylene. Treatment of **12** with stoichiometric activators $B(C_6F_5)_3$ and $[HMe_2NPh][B(C_6F_5)_4]$ led to decomposition.[27,28] Addition of H_2 to **12** in the presence of excess PMe_3 results in clean formation of methane, isobutylene, and $Cp^*TaH_4(PMe_3)_2$ (eq 7). The tetrahydride product has been previously characterized from the hydrogenation of Cp^*TaMe_4 with PMe_3.[29] For comparison, it is known that hydrogenation of $Cp^*_2ZrMe_2$ produces the hydride species $Cp^*_2Zr(H)_2$ cleanly.[30]

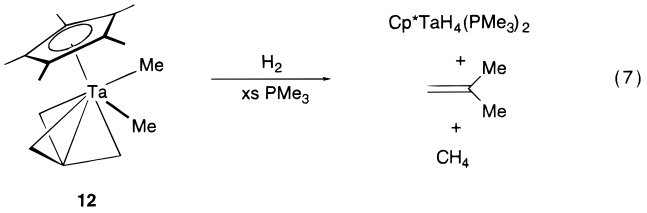

(7)

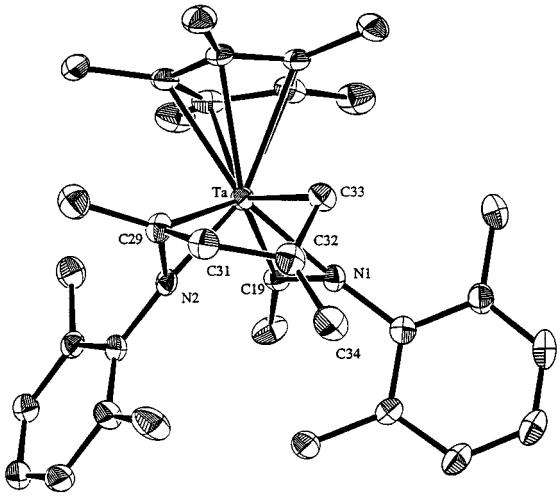

Figure 8. ORTEP drawing of **13**. Ellipsoids are drawn at 30% probability. Hydrogen atoms are omitted for clarity.

Addition of 1 equiv of $2,6\text{-}Me_2C_6H_3NC$ to **12** gives a complex mixture of products. When 2 equiv of isocyanide are added, the reaction is nearly quantitative by ^{1}H NMR spectroscopy.[31] The product **13** is characterized by one Cp* signal and six methyl groups. In addition, there are two signals in the olefin region, and four sets of doublets (J = 15 Hz for two sets, J = 8 Hz for the other two sets). These spectroscopic data, and elemental analysis, are consistent with double isocyanide insertion. All attempts to incorporate only one $2,6\text{-}Me_2C_6H_3NC$ molecule into **12** were frustrated by the fast incorporation of the second equivalent.

Single crystals of **13** suitable for X-ray crystallography were obtained by slowly cooling a concentrated diethyl ether solution. The resulting solid-state structure is shown in Figure 8, while selected bond distances and angles are given in Table 3. Upon insertion into a Ta−Me bond, one of the isocyanides forms a

(24) Sandstrom, J. *Dynamic NMR Spectroscopy*; Academic Press: New York, 1982.

(25) Modeled using the Dynmac software package written for the Macintosh computer. See: Heinekey; M. D.; Hinkle, A. S.; Close, J. D. *J. Am. Chem. Soc*. **1996**, *118*, 5353.

(26) Mayer, J. M.; Curtis, C. J.; Bercaw, J. E. *J. Am. Chem. Soc*. **1983**, *105*, 2651.

(27) For reactions of $B(C_6F_5)_3$ with dimethyl zirconocenes see: Yang, X.; Stern, C. L.; Marks, T. J. *J. Am. Chem. Soc*. **1994**, *116*, 10015.

(28) For reactions of $[HMe_2NPh][B(C_6F_5)_4]$ with dimethyl zirconocenes and zirconium alkyls see: (a) Hlatky, G. G., Turner, H. W.; Eckman, R. R. *J. Am. Chem. Soc*. **1989**, *111*, 2728. (b) Bochman, M.; Lancaster, S. J.; Hursthouse, M. B.; Abdul Malik, K. M. *Organometallics* **1994**, *13*, 2235. (c) Bochman, M.; Lancaster, S. J. *Organometallics* **1993**, *12*, 633. (d) Bochman, M. *Angew. Chem., Int. Ed. Engl*. **1992**, *31*, 1181. (e) Bochman, M.; Jaggar, A. J.; Nicholls, J. C. *Angew. Chem., Int. Ed. Engl*. **1990**, *29*, 780. (f) Bochman, M.; Karger, G.; Jaggar, A. J. *J. Chem. Soc., Chem. Commun*. **1990**, 1038.

(29) Mayer, J. M.; Wolczanski, P. T.; Santarsiero, B. D.; Olson, W. A.; Bercaw, J. E. *Inorg. Chem*. **1983**, *22*, 1149.

(30) (a) Miller, F. D.; Sanner, R. D. *Organometallics* **1988**, *7*, 818. (b) Lin, Z.; Marks, T. J. *J. Am. Chem. Soc*. **1987**, *109*, 7979. (c) Jordan, R. F.; Bajgur, C. S.; Dasher, W. E.; Rheingold, A. L. *Organometallics* **1987**, *6*, 1041.

(31) For other examples of $2,6\text{-}Me_2C_6H_3NC$ insertion into Ta−Me bonds see: (a) Galakhov, M. V.; Gomez, M.; Jimenez, G.; Royo, P. *Organometallics* **1995**, *14*, 2843. (b) Galakhov, M. V.; Gomez, M.; Jimenez, G.; Penlinghelli, M. A.; Royo, P. *Organometallics* **1995**, *14*, 1901. For reactions of isocyanide insertion into Cp_2ZrR_2, see (c) Bristow, G. S.; Lappert, M. F.; Atwood, J. L.; Hunter, W. E. in *Comprehensive Organometallic Chemistry*; Wilkinson, G. W., Stone, F. G. A., Abel, K. W., Eds.; Pergamon: Oxford, 1982; Chapter 23, p 600.

Table 3. Selected Bond Distances and Angles for **13**

atoms	distance (Å)	atoms	angles (deg)
Ta−N(1)	2.160(5)	Ta−C(33)−C(32)	105.0(5)
Ta−C(19)	2.150(6)	Ta−N(2)−C(29)	79.6(4)
Ta−N(2)	1.973(5)	Ta−C(29)−C(30)	131.2(5)
Ta−C(29)	2.216(7)	C(31)−C(32)−C(33)	110.4(6)
Ta−C(33)	2.219(7)	C(33)−C(32)−C(34)	124.8(8)
N(2)−C(29)	1.426(8)	C(34)−C(32)−C(31)	124.6(8)
N(1)−C(19)	1.268(8)		
C(32)−C(33)	1.47(1)		
C(32)−C(31)	1.50(1)		
C(32)−C(34)	1.33(1)		

typical iminoacyl ligand containing N(1) and C(19). The second isocyanide is part of an unusual metallabicyclic unit containing an amido moiety (Ta−N(2) = 1.973(5) Å). The distances within this fragment are consistent with two single bonds (C(31)−C(32) = 1.50(1), C(32)−C(33) = 1.47(1) Å) and one double bond (C(32)−C(34) = 1.33(1) Å). Based on the similar coupling constants, it is apparent that the four sets of doublets are due to the H atoms on C(31) and C(33), while the olefinic signals originate from the two H atoms on C(34). The structure of **13**, as shown in eq 8, is consistent with both solid state and solution data.

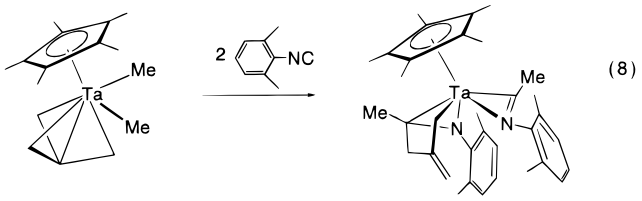

(8)

12 **13**

The metallabicyclic fragment probably forms by initial insertion of isocyanide to give an iminoacyl group, followed by nucleophilic attack by one of the methylene carbons of TMM onto the iminoacyl C_α. In the case of Cp_2ZrR_2[31c] and Cp*[C_4H_4B−N(CHMe$_2$)$_2$]TaMe$_2$,[9] isocyanide insertion occurs only into the σ ligands within the metallocene wedge.

Addition of ethylene to solutions of **6**, **7**, or **8** with MAO results in a sudden temperature increase and the formation of polyethylene. Complex **5** could not be used in these test reactions because it is insoluble in hydrocarbon solvents. Long-term stability of the active species is an important concern since many metallocene-based catalysts show thermal degradation.[32] Gas uptake measurements show that catalysts derived from **6**−**8** decompose within minutes after activation. Well-defined cationic species could not be observed using stoichiometric activators such as $B(C_6F_5)_3$ and $[HMe_2NPh][B(C_6F_5)_4]$. Combining **5**−**8** with either of these reagents did not provide polymerization catalysts. Analysis of these reactions by ^{1}H NMR spectroscopy fails since oily mixtures form which phase separate from the solvent.

Electronic Structure Calculations. As noted earlier, the TBM framework eclipses the monodentate ligands in (*t*-Bu-TBM)TaMe$_3$ (**2**), (TBM)TaMe$_2$Cl (**3**), and (TBM)Ta(NPh$_2$)Me$_2$ (**4**). The eclipsed conformation seems counterintuitive on steric grounds and is in marked contrast to the staggered conformation observed for (TMM)Fe(CO)$_3$. The eclipsed conformation of the TBM complexes of d^0 Ta(V) complexes, even in the presence of a bulky diphenylamido ligand, suggests an electronic origin for the conformation. We have used Fenske−Hall approximate MO calculations[33] and density functional theory via the Amsterdam Density Functional (ADF) implementation[34] to explore these observations further. Specifically, we will compare the bonding and geometric preference in the known Fe(II) complex (TMM)Fe(CO)$_3$ (**A**) to those in the model Ta(V) complex (TMM)TaMe$_3$ (**B**).

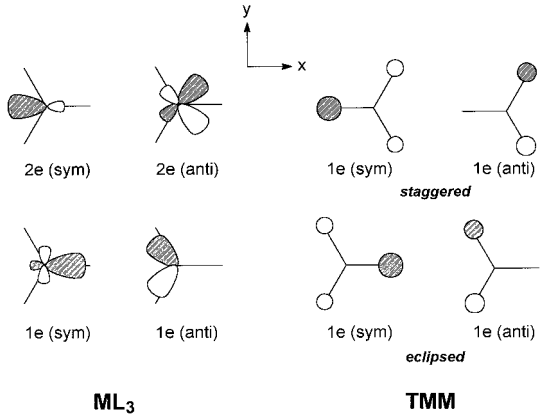

Figure 9. Projection representations of the frontier orbitals of e symmetry for a pyramidal ML$_3$ fragment and a TMM ligand. *Sym* and *anti* indicate symmetry or antisymmetry with respect to the *xz* plane.

(TMM)ML$_3$ Frontier Orbitals. Because the TBM ligand in the structures of **2**−**4** are "domed", we will consider first the relevant orbitals of a domed (C_{3v}) TMM ligand. As expected, the primary interactions between a TMM ligand and a metal atom are via the π orbitals of the ligand. The π molecular orbitals of a C_{3v} TMM ligand are the 1a$_1$, 1e, and 2a$_1$ MOs; if the ligand is considered to be a six-π-electron (TMM)$^{2-}$ ligand, then the nondegenerate 1a$_1$ and doubly degenerate 1e MOs are filled, the latter being the HOMO of the dianionic ligand. The filled 1a$_1$ MO and the 2a$_1$ LUMO are axially symmetric and cannot contribute to a rotational preference for a staggered or eclipsed geometry. Thus, our discussion will focus on the interactions between the 1e MO of the (TMM)$^{2-}$ and a d^6 [Fe(CO)$_3$]$^{2+}$ or a d^0 [TaMe$_3$]$^{2+}$ fragment. The frontier orbitals of a trigonal pyramidal ML$_3$ fragment have been previously described by many groups.[35] The d-based orbitals of a pyramidal ML$_3$ fragment adopt a familiar "three-below-two" splitting pattern, consistent with its octahedral parentage. The lower set of orbitals consists of a$_1$ and e orbitals, the lobes of which point between the extensions of the M−L bonds to the "top" of the fragment. The upper set of orbitals is an e set that has lobes that lie along the M−L bond extensions. A qualitative picture of the lower (1e) and upper (2e) sets of d-based e orbitals, projected along the 3-fold axis of the ML$_3$ fragment, is shown in Figure 9. These orbitals are labeled as *sym* or *anti* to indicate symmetry or antisymmetry with respect to a vertical mirror plane that contains one of the M−L bonds (the *xz* plane in the coordinate system of the figure).

Figure 9 also shows representations of the 1e set of π orbitals of the TMM ligand, in eclipsed and staggered conformations relative to the ML$_3$ fragment. The comparison of the "match" of the TMM 1e π orbitals with the metal-based e orbitals is

(32) Reddy, S. S.; Sivaram, S. *Prog. Polym. Sci.* **1995**, *20*, 309.

(33) Hall, M. B.; Fenske, R. F. *Inorg. Chem.* **1972**, *11*, 768.

(34) (a) Amsterdam Density Functional program, versions 1.1, 2.0, and 2.1, Theoretical Chemistry, Vrije Universiteit, Amsterdam. (b) Baerends, E. J.; Ellis, D. E.; Ros, P. *Chem. Phys.* **1973**, *2*, 41. (c) te Velde, G.; Baerends, E. J. *J. Comput. Phys.* **1992**, *99*, 84.

(35) See, for example: (a) Elian, M.; Chen, M. M. L.; Mingos, D. M. P.; Hoffmann, R. *Inorg. Chem.* **1976**, *15*, 1148. (b) Calabro, D. C.; Hubbard, J. L.; Blevins, C. H., II.; Campbell, A. C.; Lichtenberger, D. L. *J. Am. Chem. Soc.* **1981**, *103*, 6839. (c) Albright, T. A.; Burdett, J. K.; Whangbo, M. H. *Orbital Interactions in Chemistry*; Wiley: New York, 1985.

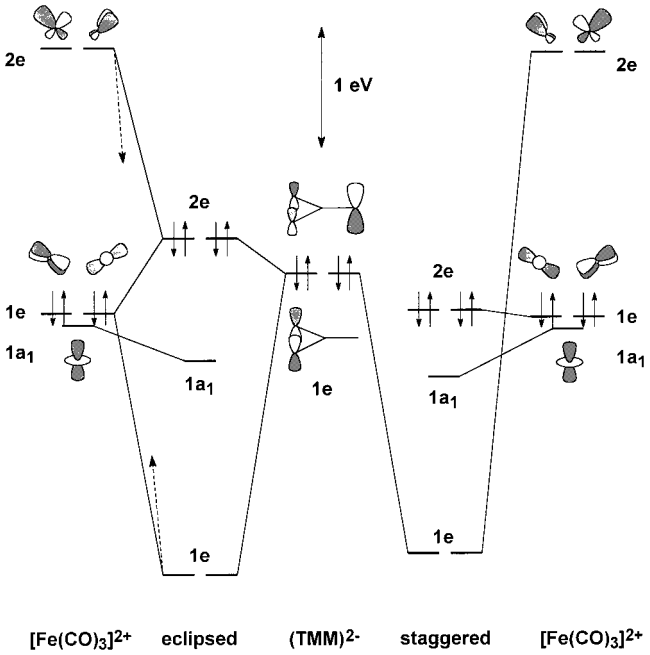

Figure 10. Frontier molecular orbital interactions in the eclipsed and staggered geometries of (TMM)Fe(CO)$_3$ (**A**).

striking and provides the first indication of the electronic source of differing rotational preference. In the eclipsed conformation, the TMM 1e π *sym* and *anti* orbitals are oriented to overlap favorably with their counterparts in the lower 1e orbitals of the ML_3 fragment. In the staggered conformation, the TMM 1e orbitals overlap better with the upper 2e orbitals of ML_3. We will see that these differences in the optimum TMM−ML_3 e interactions are key in understanding the rotational preferences in complexes **A** and **B**.

Orbital Interactions in (TMM)Fe(CO)$_3$. The bonding and rotational preference of known complex **A** have been extensively studied.[36] Our Fenske−Hall molecular orbital description of eclipsed and staggered **A**, given in Figure 10, reinforces the conclusions of these earlier studies. Consistent with the above discussion, only interactions between the fully occupied 1e HOMO of $(TMM)^{2-}$ and the d-based 1e and 2e orbitals of $[Fe(CO)_3]^{2+}$ are considered. In the d^6 $[Fe(CO)_3]^{2+}$ fragment, the 1e orbital is filled whereas the 2e orbital is unoccupied. In the eclipsed conformation of **A**, the TMM 1e orbital interacts primarily with the 1e orbital of $[Fe(CO)_3]^{2+}$. This unfavorable filled-filled interaction results in destabilization of the 2e HOMO of the complex.

Rotation of the TMM ligand to a staggered conformation relative to the $[Fe(CO)_3]^{2+}$ fragment switches the primary interaction of the TMM 1e orbital from the 1e to the 2e orbital of $[Fe(CO)_3]^{2+}$, as is evident from the percent compositions of the 1e and 2e MOs of **A** in the two conformations (Table 4). Whereas the 2e HOMO of eclipsed **A** is antibonding because of the filled-filled interaction, the 2e HOMO of staggered **A** is essentially nonbonding and is therefore at lower energy. The stabilization of the HOMO of staggered **A** relative to eclipsed **A** provides an electronic preference for the staggered conformation in addition to the evident steric preference.

The strong bonding interaction of the 1e orbital of $(TMM)^{2-}$ with the 2e orbital of $[Fe(CO)_3]^{2+}$ in staggered **A** leads to

(36) (a) Albright, T. A. *Trans. Am. Crystallogr. Assoc.* **1980**, *16*, 35. (b) Albright, T. A.; Hofmann, P.; Hoffmann, R. *J. Am. Chem. Soc.* **1977**, *99*, 7546. (c) Branchadell, V.; Deng, L.; Ziegler, T. *Organometallics* **1994**, *13*, 3115.

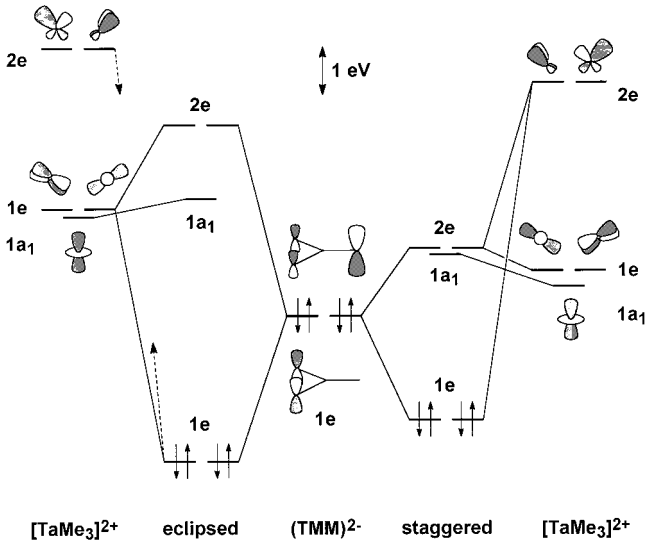

Figure 11. Frontier molecular orbital interactions in the eclipsed and staggered geometries of (TMM)TaMe$_3$ (**B**).

stabilization of the formally Huckel antiaromatic (4 π electron) TMM ligand. This situation is reminiscent of the stabilization of cyclobutadiene in (η^4-C_4H_4)Fe(CO)$_3$, an effect we have called "metalloaromaticity."[37]

Orbital Interactions in (TMM)TaMe$_3$. The bonding in (TBM)TaMe$_3$, **1**, was investigated using the model complex (TMM)TaMe$_3$, **B**. A Fenske−Hall MO diagram for complex **B** in eclipsed and staggered geometries is given in Figure 11. The most obvious difference in the electronic structures of **A** and **B** is the d^0 electron count for the $[TaMe_3]^{2+}$ fragment of **B**. As a consequence, both the 1e and 2e orbitals of the metal fragment are empty and available for bonding interactions with the filled 1e orbitals of $(TMM)^{2-}$.

In eclipsed **B**, the $(TMM)^{2-}$ 1e orbitals interact significantly with the empty 1e, and, to a lesser extent, the 2e orbitals of $[TaMe_3]^{2+}$, yielding the strongly bonding 1e HOMO of the complex (Table 4). In staggered **B**, the 1e orbitals of $[TaMe_3]^{2+}$ have almost zero overlap with the TMM ligand, and the primary interaction in the 1e HOMO of the complex is between the 1e orbitals of $(TMM)^{2-}$ and the 2e orbitals of $[TaMe_3]^{2+}$. The 2e orbitals of $[TaMe_3]^{2+}$ are energetically farther from the $(TMM)^{2-}$ 1e orbitals than are the 1e orbitals of $[TaMe_3]^{2+}$. As a result, the stabilization of the HOMO is considerably diminished relative to the eclipsed conformation. The greater stabilization of the HOMO is the electronic driving force for the seemingly nonintuitive eclipsed conformation.

The electronic driving force for the preferred eclipsed conformer of **B** is similar to that which leads to an eclipsed conformation in the d^0 complex WMe_6. In an elegant treatment of Group VI MX_6 complexes, Albright et al. invoked the second-order Jahn−Teller theorem to propose that WMe_6 adopts a trigonal prismatic geometry in preference to a more intuitive octahedral geometry.[38] Our orbital explanation here for **B** is analogous to the one that they used for WMe_6: By adopting an eclipsed geometry, the lower set of empty metal-based e orbitals in the MMe_3^{2+} fragment can be utilized more effectively as acceptors of ligand charge than in an octahedral geometry and are thus destabilized farther in energy from the filled molecular orbitals.

Density Functional Calculations. Although the Fenske−

(37) Bursten, B. E.; Fenske, R. F. *Inorg. Chem.* **1979**, *18*, 1760.
(38) Kang, S. K.; Tang, H.; Albright, T. A. *J. Am. Chem. Soc.* **1993**, *115*, 1971.

Table 4. Fenske−Hall Energies and Percent Contributions for the 1e and 2e Frontier Molecular Orbitals of Staggered and Eclipsed (TMM)$Fe(CO)_3$ and (TMM)$TaMe_3$

	(TMM)$Fe(CO)_3$ staggered		(TMM)$Fe(CO)_3$ eclipsed		(TMM)$TaMe_3$ eclipsed		(TMM)$TaMe_3$ staggered	
	1e MO	2e MO	1e MO	2e MO	1e MO	2e MO	1e MO	2e MO
MO energy, eV	−11.02	−8.89	−11.11	−8.28	−13.80	−6.40	−12.89	−9.28
% $ML_{3\ 1e}$	1.6	96.6	31.2	57.9	25.9	53.2	2.4	94.0
% $ML_{3\ 2e}$	36.8	0.3	15.0	33.0	8.0	38.8	29.9	4.0
% TMM 1e	59.3	1.5	47.0	6.7	64.6	6.5	56.9	0.3

Table 5. Relative Energies and Selected Calculated Geometric Parameters of the Staggered and Eclipsed Conformations of (TMM)$Fe(CO)_3$ (**A**) and (TMM)$TaMe_3$ (**B**)

	(TMM)$Fe(CO)_3$ staggered[a]	(TMM)$Fe(CO)_3$ eclipsed	(TMM)$TaMe_3$ eclipsed[b]	(TMM)$TaMe_3$ staggered
rel energy, kJ/mol	0	64	0	26
M−L, C	1.74 (1.81)	1.72	2.16 (2.19)	2.19
M−C_c, C[c]	1.93 (1.94)	1.94	2.23 (2.20)	2.28
M−C_t, C[c]	2.11 (2.13)	2.15	2.33 (2.33)	2.43
L−M−L, deg	100 (99)	99	102 (97)	116

[a] Averaged experimental values from ref 14c are given in parentheses. [b] Averaged experimental values from the structure of **2** (ref 11) are given in parentheses. [c] C_c is the central carbon atom of the TMM ligand; C_t is one of the terminal carbon atoms of the TMM ligand.

Hall method yields useful molecular orbitals and charge distributions, it cannot be used reliably to calculate the geometries of molecules.[39] Therefore, we used density functional calculations to estimate the rotational barriers in complexes **A** and **B**.[40] The rotational barriers were determined as the difference in total energy between the C_{3v}-optimized geometries of the eclipsed and staggered conformers of each molecule. Table 5 gives some of the geometric parameters from the optimized structures of **A** and **B** in staggered and eclipsed conformations. For staggered **A** and eclipsed **B**, the calculated geometries are compared to the experimental structures of (TMM)$Fe(CO)_3$[14c] and **2**.[11]

The calculated rotational barrier for **A** is 64 kJ/mol, in reasonable accord with the experimental value for derivatives of **A** ($\Delta G^{\ddagger} \sim 70-75$ kJ/mol)[41] and consistent with previously calculated values.[36] The calculated geometric parameters are in good agreement with those from the experimental structure.[42] Notably, the geometry of the $Fe(CO)_3$ fragment and the Fe−TMM distances are nearly invariant between the two conformers; the rotation of the TMM ligand in **A** is essentially a pure rotation of the ligand with minimal geometric reorganization of the molecule.

The rotational barrier for **B** was found to be 26 kJ/mol, considerably less than that for **A**. Significantly, the geometry of the $TaMe_3$ fragment changes drastically between the two conformers. In particular, the calculated Me−Ta−Me angles in **B** increase markedly (from 102° to 116°) as the TMM ligand is rotated from the favorable eclipsed conformation to the unfavorable staggered conformation. It is the ability of the $TaMe_3$ fragment to respond and reorient that leads to the much lower rotational barrier in **B** relative to **A**, as we will now briefly discuss.

Figure 12 shows the variation of the relative density functional energies of the d^6 $[Fe(CO)_3]^{2+}$ and d^0 $[TaMe_3]^{2+}$ fragments as a function of the L−M−L angle, denoted θ. The $[Fe(CO)_3]^{2+}$ fragment has minimum energy at θ near 90°, and the energy rises rapidly as θ increases above 100°. At the 90° angle, there

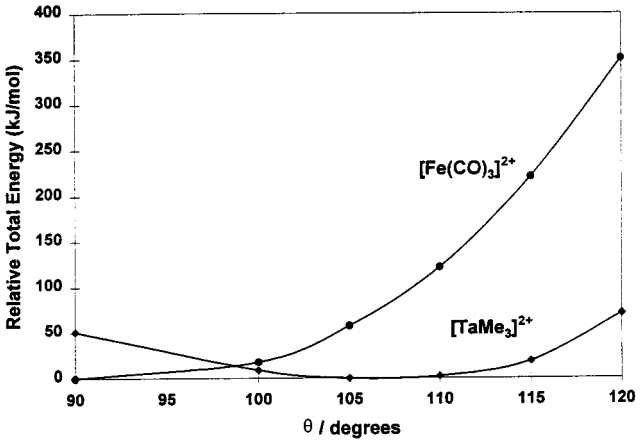

Figure 12. Variation of the total energy of the d^6 $[Fe(CO)_3]^{2+}$ and d^0 $[TaMe_3]^{2+}$ ML_3 fragments as a function of θ, the L−M−L angle.

is a minimum in the competition between the CO ligands for back-bonding interactions with the Fe $3d\pi$ orbitals.[35a] The stabilization due to back-bonding is a more important factor in the geometry of the fragment than is the steric interaction between the CO ligands.

On the basis of VSEPR considerations, the d^0 $[TaMe_3]^{2+}$ fragment might be expected to adopt a trigonal planar conformation with $\theta = 120°$. Instead, Figure 12 indicates that this fragment has a shallow potential surface with a minimum energy at $\theta = 108°$. A similar preference for pyramidalization has been seen in theoretical studies of other d^0 MX_3 fragments, such as ScH_3, $[TiH_3]^+$, and $[TiMe_3]^+$.[43] In fact, Jolly and Marynick found the optimized Me−Ti−Me angle in $[TiMe_3]^+$ to be 109°,[43a] virtually the same as we find here for $[TaMe_3]^{2+}$. This nonintuitive distortion in these d^0 fragments can be viewed as a result of attempting to maximize the donation from the methyl ligands to the metal d orbitals; in particular, a reduction of symmetry from trigonal planar to trigonal pyramidal facilitates donation into the doubly degenerate (d_{xz}, d_{yz}) metal orbitals, increasing the overall ligand-to-metal donation.

The pyramidalization of the $[TaMe_3]^{2+}$ fragment leads to mixing of the ($d_{x^2-y^2}$, d_{xy}) and (d_{xz}, d_{yz}), which generates the

(39) Bursten, B. E. *Pure Appl. Chem.* **1991**, *63*, 839.
(40) For a review of density functional theory applied to organometallic molecules, see: Ziegler, T. *Chem. Rev.* **1991**, *91*, 651.
(41) Magyar, E. S.; Lillya, C. P. *J. Organomet. Chem.* **1976**, *116*, 99.
(42) Our calculated geometric parameters vary slightly from those reported by Ziegler et al. (ref 36c) due to slight differences in basis sets and levels of optimization.
(43) (a) Jolly, C. A.; Marynick, D. S. *Inorg. Chem.* **1989**, *28*, 2893. (b) Kaupp, M.; Schleyer, P. v. R. *J. Phys. Chem.* **1992**, *96*, 7316. (c) Siegbahn, P. E. M. *J. Phys. Chem.* **1993**, *97*, 9096.

hybridized 1e and 2e sets depicted in Figure 9. In the unfavorable staggered conformation of **B**, the TMM ligand cannot effectively utilize these hybrids, so the $[TaMe_3]^{2+}$ fragment responds by, in essence, "unhybridizing" itself via flattening out. By so doing, the TMM ligand can interact preferentially with the vertically oriented (d_{xz}, d_{yz}) orbitals, which is preferable to interacting with the hybrids for the unfavorable conformer. The effect of this response of the metal fragment to the rotational barrier of the molecule is striking: A calculation of the rotational barrier of **B** with the $[TaMe_3]^{2+}$ fragment fixed at the optimized geometry in the eclipsed conformation yields a value of 160 kJ/mol, more than six times greater than the value obtained when both conformers are optimized.

In summary, there is clearly an electronic source for the preference of d^0 (TBM)TaX_3 complexes to adopt an eclipsed, rather than staggered, conformation. However, the relative softness of the potential surface for distortion of the molecule leads to much lower rotational barriers than those observed in more electron-rich systems, such as (TMM)$Fe(CO)_3$.

Summary and Conclusion

We have demonstrated that TBM−Ta compounds are easily prepared via salt metathesis routes. The piano stool compounds **1**−**4** prefer eclipsed geometries. This structural arrangement is favored over the staggered isomer even when a large, π-donating ligand is present, as in the case of **4**. Metallocene mimics, as shown by the structures of **7** and **8**, show the expected bent-sandwich geometry with TBM replacing one of the Cp ligands. Despite these structural similarities, the TBM ligand is more reactive than Cp and participates in hydrogenation and insertion reactions at rates competitive with the Ta−CH_3 bond. We attribute this reactivity to the greater σ character of the bond between Ta and the outer carbons in TMM (or TBM). The same σ character relates the eclipsed conformation of complexes such as (TBM)$TaMe_3$ to the trigonal prismatic structure of WMe_6. In the case of Cp−Ta the bonding interaction contains more π character and thus it is expected to be more inert. For these reasons, TMM and TBM are poor dianionic surrogates for Cp, at least with d^0 metals.

Compounds **9**−**11** demonstrate that TBM can accommodate a continuum of bonding modes. This property allows it to donate between four to six electrons and gives the ligand the ability to respond to the steric and electronic demands of the metal. Such bonding flexibility is potentially useful in catalytic applications where vacant sites need to be generated for the substrate to coordinate to the metal and is analogous to the η^5−η^3 ring slip distortion observed for the cyclopentadienyl ligand.

Finally, the electronic structure calculations on the model complex (TMM)$TaMe_3$ demonstrate that the eclipsed conformation adopted by compounds **2**−**4** is a consequence of preferential interactions between the filled 1e π orbitals of the $(TMM)^{2-}$ with the empty 1e orbitals of the $[TaMe_3]^{2+}$ fragment. The rotational preference of this d^0 complex differs from that of the d^6 complex (TMM)$Fe(CO)_3$ because in the latter, the 1e orbital of the $[Fe(CO)_3]^{2+}$ fragment is filled and is unavailable as an acceptor orbital. The pyramidal[44] flexibility of the $[TaMe_3]^{2+}$ fragment leads to a low calculated rotational barrier (26 kJ/mol) in (TMM)$TaMe_3$.

Experimental Section

General Considerations. All manipulations were carried out using either high-vacuum or glovebox techniques as described previously.[45] ^1H and ^{13}C NMR spectra were recorded using a Bruker AMX-400 NMR spectrometer at 400.1 and 100.6 MHz, respectively. Toluene, pentane, diethyl ether, and tetrahydrofuran were distilled from benzophenone ketyl. Elemental analyses were carried out by Desert Analytics. The preparations of Cp*(TMM)$TaMe_2$,[26] Li_2(TBM)$(TMEDA)_2$,[46] Li_2(*t*-BuTBM)$(TMEDA)_2$, and Li_2(TMM)$(TMEDA)_2$,[47] are available in the literature. MAO was purchased from AKZO Chemicals (toluene, 6.4 wt % Al, type 4).

(TBM)$TaMe_3$ (1). To a benzene solution of $Ta(CH_3)_3Cl_2$ (5.42 g, 18.2 mmol) is added dropwise Li_2(TBM)$(TMEDA)_2$ (9.65 g, 18.2 mmol) in benzene and allowed to react for 1 h. The reaction mixture is filtered through Celite, and the black solids are washed with a minimum amount of benzene. The filtrate is brought to dryness and redissolved in 30 mL of xylenes. The solvent is then evaporated under vacuum, and the remaining solids are warmed to 60 °C while under at full vacuum for an additional 1h. The remaining solids were extracted with benzene, and the xylene dissolution and evaporation are repeated. This procedure is followed with a second benzene extraction. The product purification is achieved by solvent removal, suspension over pentane, and filtration to provide an orange solid in 44% (4.12 g). ^1H NMR δ ($CDCl_3$) 7.45 (d, 6H, *o*-Ph), 7.31 (t, 6H, *m*-Ph), 7.08 (t, 3H, *p*-Ph), 4.41 (s, 3H, PhC*H*-), 0.79 (s, 9H, Ta(CH_3)$_3$); ^{13}C NMR δ ($CDCl_3$) 139.4, 128.4, 127.8, 125.8, 116.2, 102.1 (TBM), 73.3 Ta(*C*H_3)$_3$. Anal. Calcd for $C_{25}H_{27}Ta$: C, 59.05; H, 5.36. Found: C, 59.50; H, 5.41.

(*tert*-Bu-TBM)$TaMe_3$ (2). To a diethyl ether solution of $Ta(CH_3)_3Cl_2$ (2.54 g, 8.50 mmol) is added dropwise Li_2(*tert*-Bu-TBM)$(TMEDA)_2$ (5.00 g, 8.50 mmol) in diethylether−THF (9:1), and the resulting mixture is allowed to stir for 1 h. The solvent is then removed and the resulting solid extracted with pentane. Residual TMEDA can be removed by dissolving the product in octane followed by reevaporation. It may be necessary to repeat this step one more time if retention of TMEDA persists. This procedure affords (*tert*-Bu-TBM)$TaMe_3$ as an orange solid in 25% yield (1.19 g). ^1H NMR δ ($CDCl_3$) 7.36 (d, 6H, *o*-Ph), 7.23 (t, 6H, *m*-Ph), 7.00 (t, 2H, *p*-Ph), 4.34 (s, 2H, PhC*H*), 4.26 (s, 1H, t-Bu-PhC*H*), 1.27 (s, 9H, t-Bu), 0.70 (s, 9H, Ta(CH_3)$_3$); ^{13}C NMR δ ($CDCl_3$) 148.0, 139.5, 136.3, 128.4, 128.1, 127.7,125.8, 124.6, 116.1 (TBM), 102.4, 102.1, 102.0 (Ph*C*H) 73.0 Ta(*C*H_3)$_3$, 34.3 (*C*$(CH_3)_3$), 31.5 (C(*C*H_3)$_3$). Anal. Calcd for $C_{25}H_{27}Ta$: C, 61.70; H, 6.24. Found: C, 61.54; H, 6.32.

(TBM)$TaClMe_2$ (3). $ZnCl_2$ in THF (0.536 g, 3.93 mmol) is added to a stirring benzene solution of **1** (0.500 g, 0.98 mmol). The volatiles are removed in vacuo, and the product is extracted with a minimum amount of toluene. The solvent is then evaporated and the residue suspended in 1,2-dimethoxyethane. Filtration of the resulting orange precipitate provides the (TBM)$TaClMe_2$ in 63% yield (0.328 g). ^1H NMR δ (C_6D_6) 7.36 (d, 6H, *o*-Ph), 7.12 (t, 6H, *m*-Ph), 6.88 (t, 3H, *p*-Ph), 4.50 (s, 3H, PhC*H*-), 0.91 (s, 3H, Ta(CH_3)$_2$), 0.82 (s, 3H, Ta-(CH_3)$_2$) ^{13}C NMR δ (C_6D_6) 138.8, 129.3, 128.1, 127.2, 107.1, 102.8 (TBM); 72.57, 70.63 Ta(*C*H_3). Anal. Calcd for $C_{24}H_{24}TaCl$: C, 54.50; H, 4.58. Found: C, 54.14; H, 4.47.

(TBM)$TaMe_2(NPh_2)$ (4). To a THF solution of **3** (0.20 g, 0.38 mmol) is added $LiNPh_2$ (66 mg 0.38 mmol) in THF and stirred for 1 h. Solvent removal, extraction with toluene, and a pentane wash affords the product as a red solid (0.208 g, 83%). ^1H NMR: δ (C_6D_6) 7.41 (d, 6H, Ph), 7.17 (m, 8H, Ph), 6.91(m, 8H, Ph), 6.61 (t, 3H, *p*-Ph), 4.86 (s, 3H, (PhC*H*)$_3C^{2-}$), 1.14 (s, 3H, Ta−CH_3), 0.23 (s, 3H, Ta−CH_3); ^{13}C NMR: δ (C_6D_6) 144.6, 143.6 (Ph), 139.9 (PhCH)$_3C^{2-}$), 130.2, 129.5, 128.6, 128.1, 126.1, 125.4, 124.5, 121.5, 121.1, 118.1 (Ph), 100.0 (Ph*C*H)$_3C^{2-}$), 68.5 (Ta-*C*H_3), 62.8 (Ta-*C*H_3). Anal. Calcd for $TaC_{36}H_{34}N$: C, 65.35; H, 5.19; N, 2.11. Found: C, 64.90; H, 5.01; N, 1.92.

Cp(TBM)$TaMe_2$ (5). To a stirring solution of **3** (0.350 g, 0.663 mmol) in THF, is added LiCp (0.050 g, 0.694 mmol) also in THF, and

(44) Collman, J. P.; Hegedus, L. S.; Norton, J. R.; Finke, R. G. *Principles and Applications of Organotransition Metal Chemistry*; University Science Books, Mill Valley, CA, 1987; Chapter 4.

(45) Burger, B. J.; Bercaw, J. E. In *Experimental Organometallic Chemistry*; Wayda, A. L., Darensbourg, M. Y., Eds.; ACS Symp. Ser. 353; American Chemistry Society, Washington, D.C., 1987.

(46) (a) Wilhelm, D.; Clark, T.; Schleyer, P. v. R.; Buckl, K.; Boche, G. *Chem. Ber.* **1983**, *116*, 1669. (b) Wilhelm, D.; Dietrich, H.; Clark, T.; Mahdi, W.; Kos, A. J.; Schleyer, P. v. R. *J. Am. Chem. Soc.* **1984**, *106*, 7279. (c) Wilhelm, D.; Clark, T.; Schleyer, P. von. R. *J. Chem. Soc., Perkin Trans. 2* **1984**, 915.

(47) Jones, M. D.; Kemmett, R. D. W. *Adv. Organomet. Chem.* **1987**, *27*, 279.

the resulting solution is stirred for 2 h. During this period a red precipitate appears. The volume is then reduced by one-half and cooled for 1 h at −30 °C to induce further precipitation. The product is filtered as a red solid in 54% yield (0.200 g) through a fine fritted funnel. ^{1}H NMR δ (THF-d_8) 7.25 (d, 6H, *o*-Ph), 7.16 (t, 6H, *m*-Ph), 6.95 (t, 3H, *p*-Ph), 5.31 (s, 5H, C_5H_5), 4.41 (s, 3H, PhC*H*-), 0.186 (s, 6H, Ta(CH_3)$_2$); ^{13}C NMR δ (THF-d_8) 143.1, 129.5, 128.6, 125.0, 112.8, 99.1 (TBM), 119.8 (C_5H_5), 48.3, 45.9 (Ta(CH_3)$_2$). Anal. Calcd for $C_{29}H_{29}$Ta: C, 62.35; H, 5.24. Found: C, 62.20; H, 5.26.

Cp*(TBM)TaMe$_2$ (6). To a stirring solution of **3** (0.200 g, 0.378 mmol) in THF, is added LiCp* (0.054 g, 0.378 mmol) in THF and stirred for 2 h. The THF is removed, and the resulting solids are extracted with benzene. The solvent is then removed and the residue suspended in pentane. Filtration of the orange-brown solids provides the final product in 51% (0.121 g) and approximately 98% purity. ^{1}H NMR δ (C_6D_6) 7.38 (s, 6H, *o*-Ph), 7.17 (t, 6H, *m*-Ph), 6.94 (t, 3H, *p*-Ph), 1.45 (s, 15H, $C_5(CH_3)_5$), 0.11, −0.44 (s, 6H, Ta(CH_3)$_2$), the -*H*CPh are broadened into the baseline; ^{13}C NMR δ ($CDCl_3$) 141.3, 129.2, 128.0, 127.7, 124.3, 117.2 (TBM), 121.8 ($C_5(CH_3)_5$) 51.3, 46.6 (Ta(CH_3)$_2$), 11.1 ($C_5(CH_3)_5$). Anal. Calcd for $C_{32}H_{33}$Ta: C, 63.23; H, 6.02. Found: C, 63.40; H, 6.24.

Cp′(TBM)TaMe$_2$ (7). To a stirring solution of **3** (0.250 g, 0.47 mmol) in tetrahydrofuran is added LiCp′ (0.041 g, 0.47 mmol in THF) and stirred for 1 h. The THF is removed in vacuo followed byproduct extraction with toluene. The solvent is removed, and the product is washed with a minimum amount of pentane (0.175 g, 65%). ^{1}H NMR: δ (C_6D_6) 7.27 (d, 6H, *o*-Ph), 7.08 (t, 6H, *m*-Ph), 6.85 (t, 3H, *p*-Ph), 5.24 (d, 1H, α-Cp′), 5.11 (dd, 1H, *β*-Cp′), 5.09 (d, 1H, α-Cp′), 4.69 (dd, 1H, *β*-Cp′), 4.37 (bs, 3H, (PhC*H*)$_3$C^{2-}), 1.75 (s, 3H, Cp-CH_3), −0.23 (s, 3H, Ta-CH_3), −0.30 (s, 3H, Ta-CH_3); ^{13}C NMR: δ (C_6D_6) 142.50 (PhCH)$_3C^{2-}$), 129.2, 124.8, 124.8, 123.7 (Ph) 112.9, 112.1, 111.5, 110.3, 108.5 (Cp′), 86.7 (Ph*C*H)$_3$C^{2-}), 48.5 (Ta-*C*H$_3$), 46.4 (Ta-*C*H$_3$), 14.4 Cp-*C*H$_3$). Anal. Calcd for $C_{30}H_{31}$Ta: C, 62.93; H, 5.47. Found: C, 62.54; H, 5.46.

(Flu)(TBM)TaMe$_2$ (8). A THF solution of LiFlu (33 mg, 0.189 mmol) is added to a THF solution of **3** (0.10 g, 0.189 mmol) to afford an intensely red solution. This mixture is stirred for 30 min at which point the solvent is removed in vacuo. The product is extracted with 30 mL of a diethyl ether/toluene mixture (1:1). The solvents are removed to provide FluTaTBM(CH_3)$_2$ as a red solid (86 mg, 69%). ^{1}H NMR: δ (C_6D_6) 7.60−6.5 (23H, aromatic H's), 5.28 (s, 1H, (C_6H_4-C*H*C_6H_4), 3.99 (s, 3H, (PhC*H*)$_3$C^{2-}), −0.83 (Ta-CH_3), −1.12 (Ta-CH_3). ^{13}C NMR: δ (C_6D_6) 141.8 (PhCH)$_3C^{2-}$), 139.8, 137.8, 129.4−119.3 (aromatic C's), 115.7 (C_6H_4*C*HC_6H_4), 88.8 (Ph*C*H)$_3$C^{2-}), 60.8 (Ta-*C*H$_3$), 52.3 (Ta-*C*H$_3$). Anal. Calcd for $TaC_{37}H_{33}$: C, 67.47; H, 5.06. Found: C, 67.96; H, 5.16.

(HBpz$_3$)TBMTaMe$_2$ (9): A THF (THF = tetrahydrofuran) solution of NaHBpz$_3$ (22 mg, 0.095 mmol) was added dropwise to **3** (50 mg, 0.095 mmol) in THF. After stirring for 1 h, the solvent was removed in vacuo, and the resulting residue was dissolved with benzene. Filtration followed by solvent evaporation affords the product in 60% yield (40 mg). Crystals suitable for X-ray and elemental analysis were grown by slow diffusion of pentane into a benzene solution of the product. ^{1}H NMR δ (C_6D_6) 7.97, 7.89, 7.87, 7.78, 7.75, 7.72 (all d, 1H ea., 3-Hpz and 5-Hpz), 7.14 (t, 6H, *m*-Ph), 7.01 (d, 6H, *o*-Ph) (6.91 (t, 3H, *p*-Ph), 6.27, 6.15, 6.08 (all t, 1H ea., 4-Hpz) 4.98 (s, 3H, (PhC*H*)$_3$C^{2-}), 0.63, 0.19 (s, 3H, Ta−CH_3). ^{13}C NMR δ (C_6D_6) 148.8 (PhCH)$_3C^{2-}$), 143.9, 143.4, 139.8, 136.8, 134.9, 134.4 (3-pz and 5-pz), 131.1, 128.7, 128.3, 121.2 (Ph), 107.4, 106.8, 106.6 (4-pz), 104.3 (Ph*C*H)$_3$C^{2-}), 80.6, 65.4 (Ta-*C*H$_3$). Anal. Calcd for $TaC_{33}H_{34}BN_6$: C, 56.16; H, 4.87; N, 11.90. Found: C, 56.03; H, 4.85; N, 11.84.

[HB(3,5-Me$_2$-1-pz)$_3$]Ta[η^2-(CHPh)$_2$C=CHPh]Me$_2$ (10). A THF solution of KHB(1,5-Me$_2$-1-pz)$_3$ (32 mg, 0.095 mmol) was added dropwise to **3** (50 mg, 0.095 mmol) in THF. After stirring for 1 h, the solvent was removed in vacuo, and the resulting residue was dissolved with benzene. Filtration followed by solvent evaporation affords the product in 73% yield (55 mg). Crystals suitable for X-ray and elemental analysis were grown by slow diffusion of pentane into a benzene solution of the product. ^{1}H NMR δ (C_6D_6) 7.65 (bd, 2H, Ph), 7.40 (bd, 2H, Ph), 7.34 (s, 1H, PhC(*H*)=C(CHPh)$_2$), 7.33 (bd, 2H, Ph), 7.13 (bd, 2H, Ph), 6.98 (bm, 4H, Ph), 6.84 (t, 1H, *p*-Ph), 6.70 (t, 1H, *p*-Ph), 5.50, 5.47, 5,46 (all s, 3H ea., 4-Hpz), 2.25, 2.10, 2.05, 1.96, 1.88, 1.86 (s, 3H ea., CH_3-pz) 2.13, 2.00 (s, 1H ea., PhHC=C(C*H*Ph)$_2$), 1.42, 1.41 (s, 3H ea., Ta−CH_3). ^{13}C NMR δ (C_6D_6) 151.9, 150.9, 144.4, 143.4, 142.5, 141.4 (3-pz$_{quat}$ and 5-pz$_{quat}$), 129.4−124.7 (Ph), 109.2, 109.0, 108.9 (4-pz), 92.8, 70.8 (Ta-*C*H$_3$), 85.9, 83.8 (PhCH=C(*C*H$_2$-Ph)$_2$), 302, 27.2, 16.1, 15.4, 12.8, 12.1 (*C*H$_3$-pz). Anal. Calcd for $TaC_{39}H_{46}BN_6$: C, 59.24; H, 5.88; N, 10.62. Found: C, 59.30; H, 5.90; N, 10.52.

(H$_2$Bpz$_2$)TBMTaMe$_2$ (11). A THF solution of KHBpz$_3$ (17 mg, 0.095 mmol) was added dropwise to **3** (50 mg, 0.095 mmol) in THF. After stirring for 1 h, the solvent was removed in vacuo, and the resulting residue was dissolved with benzene. Filtration followed by solvent evaporation affords the product in 65% yield (40 mg). Crystal suitable for X-ray and elemental analysis were grown by slow diffusion of pentane into a benzene solution of the product. ^{1}H NMR _ (d^8-THF/C_6D_6, $T \geq 25$ °C) 7.50, 7.19 (bd ea., 2H ea., 3-Hpz and 5-Hpz), 7.27 (d, 6H, *o*-Ph), 7.10 (t, 6H, *m*-Ph), 6.83 (t, 3H, *p*-Ph), 5.65 (bt, 2H, 4-Hpz), 4.97 (s, 3H, (PhC*H*)$_3$C^{2-}), 0.51, 0.36 (Ta-CH_3); ^{13}C NMR _ (d^8-THF/C_6D_6, $T \geq 25$ °C) 144.1 (PhCH)$_3C^{2-}$), 137.5, 131.8, 130.0, 129.0 (3-pz and 5-pz), 130.9, 129.0, 125.4, 119.2 (Ph), 107.9, 107.4, 107.2 (4-pz), 95.4 (center of a very broad lump, (Ph*C*H)$_3$C^{2-}), 44.0, 36.7 (Ta-*C*H$_3$). Anal. Calcd for $TaC_{30}H_{32}BN_4$: C, 56.22; H, 5.05; N, 8.74. Found: C, 56.09; H, 4.80; N, 8.50.

Cp*Ta[(η^2-C(Me)NAr′][η^3-CH$_2$C=(CH$_2$)CH$_2$C(Me)NAr′] (13). A benzene solution of Cp*(η^4-TMM)TaMe$_2$ (0.100 g, 0.250 mmol) is treated with a benzene solution of 2,6-dimethylphenyl isocyanide (65 mg, 0.500 mmol) and stirred for 10 min. The solvent is replaced with a minimum amount of pentane and then filtered to remove any unreacted materials. Pentane removal provides the product in 95% (0.157 g). X-ray quality crystals were obtained by cooling a diethyl ether solution. Analytically pure crystals were obtained from chilling a pentane/toluene (9/1) solution for 4 days (−30 °C). ^{1}H NMR δ (C_6D_6) 7.15−6.84 (m, 6H, aromatic H's), 4.25, 4.19 (s, 1H each, C=CH_2), 4.03, 3.99, 2.89, 2.85, 2.28, 2.26, 2.09, 2.07 (all are s, CH_2), 2.38 (s, 6H, CH_3), 2.09, 1.89, 1.73, 1.50 (s, CH_3), 1.79 (s, 15H, $C_5(CH_3)_5$). ^{13}C NMR δ (C_6D_6) 244.9, 158.8, 139.1, 136.1, 131.6, 131.5, 129.7, 128.9, 126.2, 122.4, 113.3, 102.0 ($C_5(CH_3)_5$), 62.5, 58.5, 51.2, 24.3, 22.5, 21.4, 20.3, 19.5, 19.0, 11.7 ($C_5(CH_3)_5$). Anal. Calcd for $TaC_{34}H_{45}N_2$: C, 61.61; H, 6.86; N, 4.22. Found: C, 61.72; H, 6.72; N, 4.17.

Typical Polymerization Procedure. A 10 mg sample of **5** is dissolved in a toluene solution containing 18% MAO by weight. After degassing the mixture, 1 atm of ethylene is placed above the catalyst solution for 45 min at which point the reaction is quenched with 20 mL of 10% HCl in methanol followed by 20 mL of water. This mixture is stirred for 10 h, and the salt-free polymer is gravity-filtered and washed with methanol.

Electronic Structure Calculations. The Fenske−Hall approximate molecular orbital method[33] and Amsterdam Density Functional (ADF) program[34] were used for all calculations. For Fenske−Hall calculations: All atomic basis functions were generated by a least-squares fit of Slater-type orbitals to the atomic orbitals from Herman−Skillman atomic calculations.[48] Contracted double-ζ representations were used for the Ta 5d, Fe 3d, C 2p, and O 2p atomic orbitals. An exponent of 1.16 was used for the hydrogen 1s AOs.[49] The basis functions for Ta were derived for the +2 oxidation state with fixed 6s and 6p exponents of 2.0. The basis functions for Fe were derived from the +1 oxidation state with fixed 4s and 4p exponents of 2.0 and 1.8, respectively. The basis functions for C and O were derived from the 0 oxidation state. The 3σ and 6σ orbitals of CO were deleted from the variational orbitals.[50] The ML$_3$ fragments were given idealized L−M−L angles of 90°. For ADF calculations: The geometries of the staggered and eclipsed conformers of (TMM)Fe(CO)$_3$ were optimized using a procedure analogous to that used by Ziegler et al.,[36c] i.e., the geometries were optimized under C_{3v} symmetry at the local density approximation (LDA) level.[51] The rotation barrier was calculated with the incorpora-

(48) Bursten, B. E.; Jensen, J. R.; Fenske, R. F. *J. Chem. Phys.* **1978**, *68*, 3320.
(49) Hehre, W. J.; Stewart, R. F.; Pople, J. A. *J. Chem. Phys.* **1969**, *51*, 2657.
(50) Lichtenberger, D. L.; Fenske, R. F. *J. Chem. Phys.* **1969**, *51*, 4274.
(51) Vosko, S. H.; Wilk, L.; Nusair, M. *Can. J. Phys.* **1980**, *58*, 1200.

tion of Becke's nonlocal exchange[52] and Perdew's nonlocal correlation[53] corrections (BP). The geometry of the staggered and eclipsed structures of (TMM)$TaMe_3$ were fully optimized under C_{3v} symmetry at the BP level of calculation. The energies of the $[Fe(CO)_3]^{2+}$ and $[TaMe_3]^{2+}$ fragments at various values of θ were calculated at the BP level. A double-ζ basis set was chosen for C, O, and H, and a triple-ζ basis was used for Ta and Fe. The $1s^2$ configuration of C and O, the $1s^2$, $2s^2$, $2p^6$ for Fe, and the all atomic subshells for $n = 1$ through $n = 4$ and the 5s and 5p of Ta were assigned the core and treated by the frozen core approximation.

Crystallography. Crystals of **4**, **8** and **13** were mounted under a flow of nitrogen onto glass fibers with epoxy. These were then placed on the diffractometer (Enraf-Nonius-CAD4) in a cold nitrogen stream. Data were collected at −60 °C using a low-temperature device.

An absorption correction using the program DIFABS[54] was applied to **4**, **8**, **9**, **10**, **11**, and **13**. The structures were determined by heavy-atom Patterson methods (DIRDIF−Patty: teXsan).[55] The structures were refined using standard least squares routines. Non-hydrogen atoms were refined with anisotropic thermal parameters. Hydrogen atoms were included in idealized positions.

Crystals of **7**, **9**, **10**, and **11** were mounted on glass fibers under Paratone-8277 and placed on the X-ray diffractometer in a cold nitrogen stream supplied by a Siemens LT-2A low-temperature device. The X-ray intensity data were collected on a standard Siemens SMART-CCD Area Detector System equipped with a normal focus molybdenum-target X-ray tube operated at 1.5 kW (50 kV, 30 mA). A total of 1.3 hemispheres of data were collected using a narrow frame method with scan widths of 0.3° in ω, and an exposure time of 10 s/frame. Frames were integrated to 0.75 with the Siemens SAINT program. The space groups were assigned on the basis of systematic absences and intensity statistics by using the XPREP program.[56]

The structure of **7** was solved by direct methods using SHELXS-86 and refined by full-matrix least-squares on F^2. Non-hydrogen atoms were refined with anisotropic thermal parameters. Hydrogen atoms were included in idealized positions.

Acknowledgment. G.C.B. is an Alfred Sloan Fellow and a Henry and Camille Dreyfus Teacher Scholar. The authors are grateful to these agencies and to the Petroleum Research Foundation (ACS) for financial assistance. J.P.G. and B.E.B. acknowledge the Ohio Supercomputer Center for use of their facilities.

Supporting Information Available: Complete details for the crystallographic studies of compounds **4**, **7**, **8**, **9**, **10**, **11**, and **13** (72 pages, print/PDF). See any current masthead page for ordering information and Web access instructions.

JA981640T

(52) Becke, A. D. *Phys. Rev.* **1988**, *A38*, 2398.
(53) Perdew, J. P. *Phys Rev.* **1986**, *B33*, 8822. *Ibid.* **1986**, *B34*, 7406 (erratum).
(54) DIFABS: Walker, N.; Stuart. *Acta Crystallogr.* **1983**, *A39*, 158−166. An empirical absorption correction program.
(55) *TEXSAN*: *Single-Crystal Structure Analysis Software*. Molecular Structure Corporation, The Woodlands, TX, 1993.
(56) *SHELXTL*: *Structure Analysis Program*. 5.04; Siemens Industrial Automation, Inc.; Madison, WI, 1995.